A co-estimation framework for state of charge and parameters of Lithium-ion battery with robustness to aging and usage conditions

Natella D., IEEE Student Member, Onori S., IEEE Senior Member, and Vasca F., IEEE Senior Member

***Abstract*—Aging and usage conditions affect the battery parameters such as capacity and changes in the open-circuit voltage and internal resistance dependencies on the state of charge. This paper proposes an on-board strategy for the simultaneous estimation of these parameters and their robust evaluation during the battery life. The proposed co-estimation framework consists of a set of interconnected subsystems grounded on the integration of recursive least-squares techniques and a Luenberger-like observer which are independently designed by relying on moving averages of voltage and current measurements. Each subsystem is separately activated through logic variables which select the operating conditions proper for the estimation purposes and allows tracking of model parameters variations. The effectiveness of the proposed solution over experiments with a cylindrical LG M50T INR21700 Li-ion cell with NMC cathode and graphite/silicon anode.**

***Index Terms*—Battery management system, state of charge, state of health, experimental battery data.**

I. Introduction

Knowledge of battery degradation due to aging and usage conditions is key for energy management systems in many applications such as electric and hybrid vehicles, smart grids, satellites. Changes in the battery behavior can be captured by means of corresponding variations of its model parameters [1]. It is widely recognized that the state of health (SOH) reduction highlights the loss of the battery charge capacity and is dependent on the usage, e.g., charging/discharging patterns and on the overall cycles or ampere-hour-throughput that the battery has undergone during its life [2], [3], [4]. Degradation manifests itself not only in the SOH reduction over time, but also on variations of the open-circuit voltage (OCV) vs. state of charge (SOC) nonlinear map [5], [6]. The importance of accounting for changes in the dependence of OCV on SOC as the battery degrades has been recognized in the literature [7], [8], [9], for all ranges of SOC values [10], [11]. Another well-known effect of aging and usage conditions is the increase of the equivalent internal resistance R_0 [12] and the variations of its dependence on SOC [13], [14].

Manuscript received Month xx, 2xxx; revised Month xx, xxxx; accepted Month x, xxxx. .

Natella D. and Vasca F. are with the Department of Engineering, University of Sannio, 82100 Benevento, Italy (e-mail: {dnatella, vasca}@unisannio.it).

Onori S. is with the Department of Energy Resources Engineering, Stanford University, Stanford, CA 94305; (e-mail: sonori@stanford.edu).

The references above indicate the importance for an online identification of different parameters during the battery life and this has motivated the use of the term "co-estimation" standing for simultaneous tracking of SOC and variations of the battery parameters. The problem of real-time estimation of the battery parameters has been widely investigated in the literature either with model-free or model-based techniques. The latter approach is the one used in our study. Despite the recent progress towards the adoption of more sophisticated model-based observers [15], estimation algorithms based on equivalent circuit models (ECMs) are still the preferred solution for the design of real-time estimators thanks to their straightforward and computational friendly implementation [16]. In this paper, a novel co-estimation framework based on ECM for simultaneous online evaluation of SOC, SOH, identification of the parameters of polynomial $OCV(SOC)$ and $R_0(SOC)$ characteristics and tracking of the other equivalent circuit parameters variations during Li-ion battery life is proposed. The analysis of this "complete" co-estimation problem is still in its infancy but there exist many studies which consider co-estimation of SOC with specific subsets of the battery parameters [17], so as discussed below.

The co-estimation problem of SOC and ECM parameters has been investigated in [18] where a polynomial approximation of the $OCV(SOC)$ map with constant coefficients and a fixed capacity are used. A constant capacity is also considered in [19] where a partial least-squares algorithm is used by exploiting a step-by-step linearization of the battery voltage as a function of SOC and battery current, whose coefficients must be estimated online. The capacity is a fixed parameter also in the co-estimation approach for SOC and ECM parameters proposed in [20] where an offline identified piecewise linear approximation of the $OCV(SOC)$ map is assumed and in [14] where the coefficients of the $OCV(SOC)$ characteristic are estimated online. Unfortunately the estimation performance obtained with the latter approaches is weakened by the commutations between the different regions of SOC in the piecewise function which are fixed a priori. A co-estimation strategy based on a Wiener configuration of the ECM is presented in [21] where the capacity is assumed as a constant and the map $OCV(SOC)$ is obtained offline by averaging the curves recorded during charging and discharging phases.

Online identification of SOH based on cell voltage measurements and not just current measurements is important for

cell diagnostics and balancing, especially for hybrid electric vehicles where battery is charged while driving. Many co-estimation studies consider the battery health degradation due to aging. In [22] the SOC is obtained by using an $OCV(SOC)$ characteristic which is fixed a priori and the battery health is indirectly evaluated by exploiting the variations of the internal resistance. The same parameter is also used to compensate the $OCV(SOC)$ drift due to aging and the estimation algorithm depends on the strong assumption of having a slowly varying OCV (formally with zero time derivative). Differently from [22], the typical approach used for the online evaluation of SOH is the reduction of the battery capacity. The combined SOC/SOH estimation algorithm presented in [23] requires offline experimental procedures for SOH and internal resistance evaluations which are triggered when the relative estimation error of the voltage exceeds a threshold to be designed. A sliding-mode observer for SOC/SOH estimation has been proposed in [24] but a linear $OCV(SOC)$ characteristic is assumed except for very small values of SOC and the knowledge of the ECM parameters is required. The latter assumption is also needed for the Kalman filtering approach proposed in [25] where the model parameters are estimated offline by conducting specific driving test at the beginning of service life of the battery. The online estimation of the internal resistance is included in the SOC/SOH algorithm discussed in [26], however the resulting scheme of interlaced sliding-mode observers requires the knowledge of the slope of the $OCV(SOC)$ characteristic and some of the ECM parameters. A Kalman filter for SOC detection combined with a recursive least-squares (RLS) algorithm for the ECM parameters is proposed in [27] but the equation used for the OCV estimation requires the comparison with a pre-recorded table $OCV(SOC)$ which is not corrected online. A similar difficulty emerges from the technique proposed in [8] where the errors used for the online adaptations require data for the OCV and the battery capacity. Fractional-order models for SOC estimation with offline estimated ECM and capacity parameters are used in [28] and in [6] by including online SOH estimations with different expressions for the dependence of OCV on SOC at various aging stages but each with constant parameters. The SOC/SOH and ECM parameters co-estimation problems analyzed in [29], [30], [31] do not consider online adaptations of the OCV map which, instead, is taken into account in our solution. Possible changes of the parameters of the $OCV(SOC)$ characteristic are not considered in [32] either, where a hierarchical multi-time-scale co-estimation framework is proposed and the SOH monitoring is realized only offline at a regular interval while in our case is performed in real-time.

The problem of online estimation of the OCV has been investigated in [33] with adaptive Kalman filtering and in [34], [35] with RLS equations, where the instantaneous value of the OCV is used as a constant parameter to be estimated. A similar idea is used in [36] where two Kalman filters with the same measurement equation are integrated for the capacity and the SOC estimations together with an RLS algorithm for the ECM parameters identification. Differently from our framework, the latter solutions do not consider the fact, since the estimator runs synchronously with the battery use, the OCV cannot be assumed with zero time derivative because of the time variations of SOC. On the other hand, the parameters of the $OCV(SOC)$ curve are expected to change slower than the SOC dynamics and not all operating conditions provide useful data for the parameters estimation [8]. These aspects are exploited for the design of our co-estimation framework.

The literature analysis presented above shows that finding robust solutions to the complete co-estimation problem is still an open issue. It is worth mentioning that having an acceptable error in the SOC estimate is not enough to give up on independently tracking the parameters' changes due to aging as justified by their different meaning and use in battery management systems. This paper provides a contribution in this direction by proposing a new framework where estimators for SOC, SOH, $OCV(SOC)$ and $R_0(SOC)$ characteristics, and ECM parameters can be separately designed and simultaneously (or independently) activated while keeping the calibration effort low. Moreover, the novel implementation-related aspects of the proposed framework are:

- the design of suitable moving average functions of the measured variables designed by exploiting the time-scale separation of the estimated variables;
- the introduction of logic variables to efficiently select the operating conditions proper for the estimation.

The rest of the paper is organized as follows. In Section II the ECM of the battery under study is presented. Section III introduces the estimation framework along with its subsystems for the $OCV(SOC)$ and $R_0(SOC)$ characteristics, battery capacity, SOC and ECM parameters. The complete integrated estimator is described in Section IV. The effectiveness of the proposed solution is verified over battery experimental data and results are discussed in Section V. Finally, in Section VI conclusions are summarized.

II. Battery Dynamic Model

The typical equivalent electric circuit of an ECM is shown in Fig. 1, where i_b is the battery current assumed to be positive during discharge, e_b is the voltage at the battery terminals, v_ℓ is the voltage across the capacitor which captures the battery dynamics in the $R_\ell C_\ell$ branch, $\ell = 1, \dots, L$, OCV is the open-circuit voltage, R_0 is the equivalent internal resistance.

Applying Kirchhoff's circuit laws to the circuit of Fig. 1, by including the state of charge equation, and by discretizing the continuous-time differential equations with the backward-Euler method and a sampling period $h \in \mathbb{R}_+$, one obtains

$$v_\ell(k) = \frac{R_\ell C_\ell}{h + R_\ell C_\ell} v_\ell(k-1) + \frac{h R_\ell}{h + R_\ell C_\ell} i_b(k) \tag{1a}$$

$$SOC(k) = SOC(k-1) - \frac{h}{Q} i_b(k) \tag{1b}$$

$$e_b(k) = OCV(SOC(k)) - \sum_{\ell=1}^{L} v_\ell(k) - R_0(SOC(k)) i_b(k) \tag{1c}$$

for $\ell = 1, \dots, L$, where $k \in \mathbb{N}$ is the discrete time-step, $\mathbb{N}$ being the set of positive integers, and the initial conditions

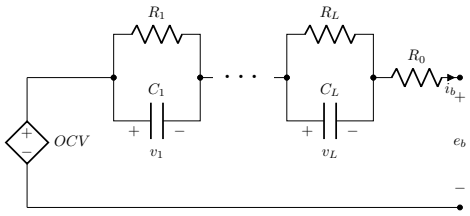

Fig. 1. Equivalent circuit model of the battery cell.

are $v_\ell(0)$ and $SOC(0)$. The model (1) is in state-space form with (1a)–(1b) being the dynamic equations of the state variables v_ℓ, $\ell = 1, \dots, L$, and SOC, the battery current i_b is the input and (1c) is the output equation. In particular, (1c) is a nonlinear function of the state variable SOC through the $OCV(SOC)$ and $R_0(SOC)$ characteristics. The typical dependence of the internal resistance R_0 on SOC motivates the approximation of a polynomial approximation in the form

$$R_0(SOC) = \sum_{j=0}^{J} b_j (SOC)^j \tag{2}$$

where $b_j \in \mathbb{R}$, $j = 0, 1, \dots, J$, $J \in \mathbb{N}$ is the desired order of approximation determined by the polynomial degree [13], [14] and $\mathbb{R}$ is the set of real numbers. The $OCV(SOC)$ map can be efficiently approximated by a polynomial function of SOC [6], [18], [21]. Specifically, one can write:

$$OCV(SOC) = \sum_{p=0}^{P} a_p (SOC)^p \tag{3}$$

where $a_p \in \mathbb{R}$, $p = 0 \dots, P$ and $P \in \mathbb{N}$ is the desired order of the polynomial.

III. Estimator Subsystems

The architecture of the proposed estimator consists of three interconnected subsystems: i) a SOC observer, ii) an RLS estimator of the parameters of the polynomial $OCV(SOC)$ and $R_0(SOC)$ characteristics and iii) an RLS estimator of the battery capacity Q.

A. SOC observer

The proposed SOC observer is obtained by using the dynamic model (1) and the error between the measured and the estimated battery voltage. To start with, for the development of the SOC estimator we assume the battery capacity Q is known. By using a Luenberger-like structure starting from the model (1)–(3), one can write

$$\begin{aligned}\hat{v}_\ell(k) =& \frac{R_\ell C_\ell}{h + R_\ell C_\ell}\hat{v}_\ell(k-1) + \frac{hR_\ell}{h + R_\ell C_\ell} i_b(k) \\ &+ g_\ell(e_b(k) - \hat{e}_b(k))\end{aligned} \tag{4a}$$

$$S\hat{O}C(k) = S\hat{O}C(k-1) - \frac{h}{Q} i_b(k) + g_{L+1}(e_b(k) - \hat{e}_b(k)) \tag{4b}$$

$$\begin{aligned}\hat{e}_b(k) =& \sum_{p=0}^{P} a_p (S\hat{O}C(k))^p - \sum_{\ell=1}^{L} \hat{v}_\ell(k) \\ &- \sum_{j=0}^{J} b_j (S\hat{O}C(k))^j i_b(k)\end{aligned} \tag{4c}$$

for $\ell = 1, \dots, L$, $k \in \mathbb{N}$, with initial conditions $\hat{v}_\ell(0)$ and $S\hat{O}C(0)$, where $\hat{v}_\ell$, $S\hat{O}C$ and $\hat{e}_b$ are the estimated values of the internal voltage, the state of charge and the battery voltage, respectively, and g_ℓ, $\ell = 1, \dots, L+1$ are the observer gains. The observer (4) has two inputs: the measured current i_b and the measured battery voltage e_b.

In the particular case $J = 0$ and $P = 1$, the model (4) is linear and the observer gains g_ℓ, $\ell = 1, \dots, L+1$ can be designed with classical techniques for linear systems. In particular, it is easy to verify that the corresponding observability matrix is full rank for almost all nonzero a_1 and h, if $R_i C_i \neq R_j C_j$ for any $i \neq j$. Therefore, a possible design rule for the observer vector gain $g \in \mathbb{R}^{L+1}$ consists of assigning the desired eigenvalues to the dynamic matrix of the observer (4).

B. Estimation of the $OCV(SOC)$ characteristic

The $OCV(SOC)$ map has been generally considered constant, i.e., not subject to aging, in the vast majority of the literature work focused on SOH estimation. In the proposed estimator, the dependence of OCV on SOC is modeled with a polynomial function whose parameters are updated and estimated upon aging via an RLS algorithm.

Before presenting the proposed estimator, we briefly recall the equations describing a generic RLS procedure. Assume that a vector $y(k) \in \mathbb{R}^m$, $m \in \mathbb{N}$, available at time-step $k \in \mathbb{N}$, can be approximated through a linear combination of $\pi \in \mathbb{N}$ unknown parameters $\hat{\theta}(k) \in \mathbb{R}^\pi$ via $\varphi(k)^\top \hat{\theta}(k)$ where $\varphi(k) \in \mathbb{R}^\pi$ is a vector of known quantities at time-step k. Indicating with $\epsilon(k) \in \mathbb{R}^m$ the model error, one can write

$$y(k) = \varphi(k)^\top \hat{\theta}(k) + \epsilon(k) \tag{5}$$

for $k \in \mathbb{N}$. By minimizing the root mean square (RMS) of the estimation error and by using a forgetting factor $\mu \in (0, 1]$, the equations describing the RLS algorithm can be written as

$$\begin{aligned}S(k) =& (1 - \delta(k))S(k-1) \\ &+ \delta(k)(\mu S(k-1) + \varphi(k)\varphi(k)^\top)\end{aligned} \tag{6a}$$

$$\gamma(k) = S(k)^{-1}\varphi(k) \tag{6b}$$

$$\hat{\theta}(k) = \hat{\theta}(k-1) + \delta(k)\gamma(k)\left(y(k) - \varphi(k)^\top \hat{\theta}(k-1)\right) \tag{6c}$$

for $k \in \mathbb{N}$, with $\hat{\theta}(0) \in \mathbb{R}^\pi$ and $S(0) \in \mathbb{R}^{\pi \times \pi}$ initial conditions of the estimator. The logic variable $\delta(k) \in \{0, 1\}$ enables the estimation of the parameters, i.e. if $\delta(k) = 0$ from (6a) it follows $S(k) = S(k-1)$ and from (6c) it is $\hat{\theta}(k) = \hat{\theta}(k-1)$ regardless of $y(k)$ and $\varphi(k)$. In particular, the variable δ allows one to exclude data corresponding to operating conditions which do not provide significant information for the estimation of the parameters. The design rule for δ is described in Sec. IV.

Equation (6c) can be interpreted as a recursive estimator of an unknown constant parameter vector, i.e., $\theta(k) = \theta(k-1)$ for all k. Note that, in the following the generic vector $\hat{\theta}(k)$ corresponds to different model parameters whether the RLS expressions (5)–(6) are applied to the estimation of the different parameters.

Let us consider the application of the RLS algorithm (5)–(6) for the estimation of the parameters of the $OCV(SOC)$

characteristic. For the sake of simplicity let us neglect for now the dependence of the internal resistance on SOC. This assumption will be removed in next subsection. From (1c), (2) with $J = 0$, i.e., $R_0(SOC) = R_0$ and (3) one can write

$$e_b(k) + R_0 i_b(k) + \sum_{\ell=1}^{L} \hat{v}_\ell(k) = \sum_{p=0}^{P} a_p (S\hat{O}C(k))^p + \epsilon_1(k) \quad (7)$$

for $k \in \mathbb{N}$, where ϵ_1 is the error corresponding to the approximation of the $OCV(SOC)$ map with the polynomial function of SOC with the desired order P.

The parameters a_p, $p = 0, 1, \ldots, p$, of the polynomial function are usually known for a fresh battery but change and therefore are unknown as the battery ages. Since aging is characterized by slow varying dynamics, the parameters can be assumed to have much slower variations as opposed to the state of charge dynamics. In order to exploit this reasonable hypothesis, we consider a filtered version of (7). In particular, by taking the moving average over N samples on both sides of (7) one can write

$$\begin{aligned}
&\frac{1}{N} \sum_{s=k-N-1}^{k} \left[e_b(s) + R_0 i_b(s) + \sum_{\ell=1}^{L} \hat{v}_\ell(s) \right] \\
&\quad = \frac{1}{N} \sum_{s=k-N-1}^{k} \left[\sum_{p=0}^{P} \hat{a}_p(s) (S\hat{O}C(s))^p + \epsilon_1(s) \right] \\
&\quad = \sum_{p=0}^{P} \frac{1}{N} \sum_{s=k-N-1}^{k} \hat{a}_p(s) (S\hat{O}C(s))^p + \frac{1}{N} \sum_{s=k-N-1}^{k} \epsilon_1(s) \\
&\quad = \sum_{p=0}^{P} \hat{\alpha}_p(k) \frac{1}{N} \sum_{s=k-N-1}^{k} (S\hat{O}C(s))^p + \epsilon_2(k) \qquad (8)
\end{aligned}$$

for $k \geq N$, where $\hat{a}_p(k)$, $p = 0, 1, \ldots, P$ are the estimations of the parameters a_p, $p = 0, 1, \ldots, P$, respectively, at the time-step k and

$$\hat{\alpha}_p(k) = \frac{1}{N} \sum_{s=k-N-1}^{k} \hat{a}_p(s) \qquad (9)$$

for $p = 0, 1, \ldots, P$. The parameters $\hat{a}_p$, $p = 0, 1, \ldots, P$, are influenced by the battery history rather than on the particular conditions over the small time interval of length N in which the moving averages are computed, see [37], [38] for a more formal analysis of these arguments. This justifies (8) where we used the slowly varying approximation for the parameters $\hat{a}_p$, $p = 0, 1, \ldots, P$ with respect to the variations of SOC, which allows one to approximate the moving average of the product $\hat{a}_p(S\hat{O}C)^p$ with the product of the moving average of each variable. The error variable ϵ_2 in (8) takes into account both this approximation and the error due to the polynomial approximation of the $OCV(SOC)$ through ϵ_1.

By taking

$$\hat{\theta}(k)^\top = \begin{pmatrix} \hat{\alpha}_0(k) & \ldots & \hat{\alpha}_P(k) \end{pmatrix}, \qquad (10)$$

the expression (8) can be written in the form (5) with

$$y(k) = \frac{1}{N} \sum_{s=k-N-1}^{k} \left[e_b(s) + R_0 i_b(s) + \sum_{\ell=1}^{L} \hat{v}_\ell(s) \right] \quad (11a)$$

$$\varphi(k)^\top = \frac{1}{N} \sum_{s=k-N-1}^{k} \begin{pmatrix} 1 & S\hat{O}C(s) & \ldots & (S\hat{O}C(s))^P \end{pmatrix} \quad (11b)$$

for $k \geq N$. The application of the RLS algorithm (5)–(6) with the definitions (10) and (11) can be extended to any $k \in \mathbb{N}$ by choosing the initial conditions $\hat{v}_\ell(\sigma)$, $\ell = 1, \ldots, L$ and $S\hat{O}C(\sigma)$ for $\sigma \in \{-N, \ldots, 0\}$. The estimate of the internal voltages $\hat{v}_\ell$, $\ell = 1, \ldots, L$, for (11a) is provided by the Luenberger-like observer.

It is interesting to note that if the coefficients a_p, $p = 0, 1, \ldots, p$ are constant, then (7) and (8) are equivalent with $\epsilon_2(k) = \frac{1}{N} \sum_{s=k-N-1}^{k} \epsilon_1(s)$. On the other hand, the $OCV(SOC)$ map is subject to changes which are reflected in drifting and variation of the parameters the OCV curve depends on. Equation (9) is motivated by the fact that one would expect that the $OCV(SOC)$ map exhibits slow variations over the moving average interval of N time-steps.

C. Online identification of the internal resistance

The RLS algorithm described above can be generalized in order to include the online estimation of the internal resistance. In particular, from (1c), (2) and (3) one can write

$$\begin{aligned}
e_b(k) + \sum_{\ell=1}^{L} \hat{v}_\ell(k) = &\sum_{p=0}^{P} a_p (S\hat{O}C(k))^p \\
&- \sum_{j=0}^{J} b_j (S\hat{O}C(k))^j i_b(k) + \epsilon_1(k) \qquad (12)
\end{aligned}$$

for $k \in \mathbb{N}$, where ϵ_1 is the error corresponding to the approximation of the $OCV(SOC)$ and $R_0(SOC)$ maps with the corresponding polynomial functions. By taking the moving average over N samples on both sides of (12) and by using (9) one can write

$$\begin{aligned}
&\frac{1}{N} \sum_{s=k-N-1}^{k} \left[e_b(s) + \sum_{\ell=1}^{L} \hat{v}_\ell(s) \right] \\
&= \sum_{p=0}^{P} \hat{\alpha}_p(k) \frac{1}{N} \sum_{s=k-N-1}^{k} (S\hat{O}C(s))^p \\
&\quad - \frac{1}{N} \sum_{s=k-N-1}^{k} \sum_{j=0}^{J} \hat{b}_j(s) (S\hat{O}C(s))^j \; i_b(s) + \epsilon_2(k) \\
&= \sum_{p=0}^{P} \hat{\alpha}_p(k) \frac{1}{N} \sum_{s=k-N-1}^{k} (S\hat{O}C(s))^p \\
&\quad - \sum_{j=0}^{J} \hat{\beta}_j(k) \frac{1}{N} \sum_{s=k-N-1}^{k} (S\hat{O}C(s))^j \; i_b(s) + \epsilon_3(k) \qquad (13)
\end{aligned}$$

where

$$\hat{\beta}_j(k) = \frac{1}{N} \sum_{s=k-N-1}^{k} \hat{b}_j(s) \qquad (14)$$

for $j = 0, 1, \ldots, J$. In order to write (13) we used the assumption that the coefficients of the polynomial function (2) are slowly varying with respect to the time interval of length N adopted for the moving average which allows to approximate the moving average of the product with the product of the moving averages. By taking

$$\hat{\theta}(k)^\top = \begin{pmatrix} \hat{\alpha}_0(k) & \ldots & \hat{\alpha}_P(k) & \hat{\beta}_0(k) & \ldots & \hat{\beta}_J(k) \end{pmatrix}, \qquad (15)$$

the expression (13) can be written in the form (5) with

$$y(k) = \frac{1}{N} \sum_{s=k-N-1}^{k} \left[e_b(s) + \sum_{\ell=1}^{L} \hat{v}_\ell(s) \right] \tag{16a}$$

$$\varphi(k) = \frac{1}{N} \sum_{s=k-N-1}^{k} \begin{pmatrix} 1 \\ S\hat{O}C(s) \\ \vdots \\ (S\hat{O}C(s))^P \\ i_b(s) \\ S\hat{O}C(s)\ i_b(s) \\ \vdots \\ (S\hat{O}C(s))^J\ i_b(s) \end{pmatrix} \tag{16b}$$

for $k \geq N$. The application of the RLS algorithm (5)–(6) with the definitions (15) and (16) can be used in alternative to (10) and (11) in order to provide an online estimation for the internal resistance too.

D. Identification of the battery capacity

The observer (4b) requires the exact knowledge of the battery capacity Q. This parameter, which defines the battery state of health, changes as the battery is cycled. In order to estimate the battery capacity we propose to use the RLS algorithm described below.

Taking the moving average over N samples on both sides of (1b) one can write

$$\begin{aligned} -\frac{1}{N} \sum_{s=k-N-1}^{k} i_b(s) &= \frac{1}{N} \left(SOC(k) - SOC(k-N) \right) Q \\ &= \frac{1}{N} \left(S\hat{O}C(k) - S\hat{O}C(k-N) \right) \hat{Q}(k) + \epsilon_3(k) \end{aligned} \tag{17}$$

for $k \geq N$, where ϵ_3 is an error which takes into account the approximation between the actual capacity Q and its estimation $\hat{Q}(k)$ at the time-step k. By taking

$$\hat{\theta}(k) = \hat{Q}(k), \tag{18}$$

the expression (17) can be written in the form (5) by choosing

$$y(k) = -\sum_{s=k-N-1}^{k} i_b(s) \tag{19a}$$

$$\varphi(k)^\top = S\hat{O}C(k) - S\hat{O}C(k-N) \tag{19b}$$

for $k \geq N$. The application of the RLS algorithm with the definitions (18) and (19) can be extended to any $k \in \mathbb{N}$ by choosing the initial conditions $S\hat{O}C(\sigma)$ for $\sigma \in \{-N, \ldots, 0\}$.

E. Identification of the circuit dynamics

In the following we assume the presence of a single RC branch in the ECM in Fig. 1. The estimation of the ECM parameters R_ℓ and C_ℓ for $\ell = 1, \ldots, L$ and $L \geq 2$ would require the use of techniques based on singular perturbations [11] which for the sake of simplicity are not considered in our analysis but could be integrated with the proposed framework by adapting the procedure described below. In particular, the parameters R_1 and C_1 are estimated by extending the typical approach which exploits the relaxation phases, i.e., when the battery current is identically zero [16]. This choice allows one to avoid the influence of the $OCV(SOC)$ and $R_0(SOC)$ maps in the identification of R_1 and C_1. By considering $L = 1$ and $i_b = 0$ in (1a) and (1c), with simple algebraic manipulations one can write

$$e_b(k) = OCV(0) - \frac{R_1 C_1}{h} (e_b(k) - e_b(k-1)). \tag{20}$$

The expression (20) is a linear regression equation in the form (5) with the parameter vector $\theta = (OCV(0)\ R_1C_1)^\top$, $y(k) = e_b(k)$, $\varphi(k)^\top = (1\ \frac{e_b(k-1)-e_b(k)}{h})$. Then, the time constant R_1C_1 can be estimated by applying an RLS algorithm with the regression (20) reactivated at the beginning of each relaxation phase. The parameter R_1 is then obtained by applying an RLS technique on the linear regression between the voltage drop and the current discontinuity for different relaxation phases.

It should be noticed that the observability of the linearized ECM holds also in the presence of two or more RC branches which motivates the possibility to use our framework also in this more general case provided that these parameters of the ECM are known or suitably estimated.

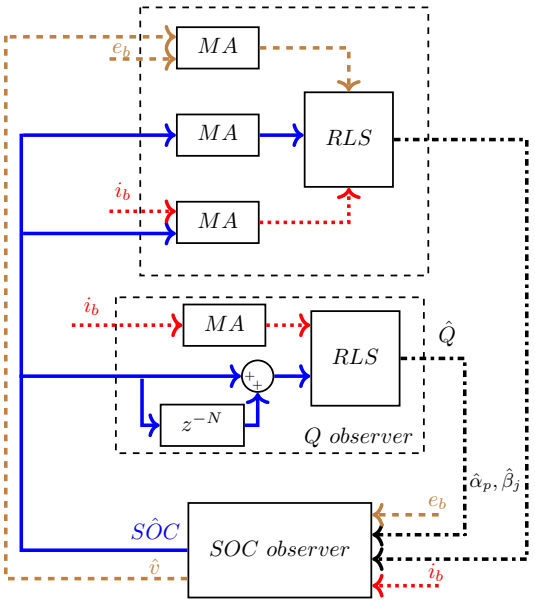

Fig. 2. Block scheme of the co-estimation framework. The inputs of the estimator are the instantaneous measured voltage e_b and current i_b; the block z^{-N} is a delay of N time-steps; the MA blocks (from top to bottom) implement the moving averages in (16a), (16b) and (19a), respectively; the RLS blocks (from top to bottom) implement the recursive least-squares algorithms (6) with (15)–(16) and (18)–(19), respectively; the SOC observer block implements (21).

IV. The Integrated Estimator

The proposed estimation scheme is shown in Fig. 2. Both the SOC observer and the two RLS estimators are characterized by dynamic elements and therefore no algebraic loops are involved in the whole scheme.

A. Subsystems interconnection

The estimation of the parameters $\hat{\alpha}_p$, $p = 0, \ldots, P$, and $\hat{\beta}_j$, $j = 0, \ldots, J$, is performed by the block scheme in the upper

side of Fig. 2 which implements (5)–(6) with (15)–(16). The inputs of this subsystem are the battery current i_b, the battery voltage e_b and the estimated state of charge $\hat{SOC}$ and voltage $\hat{v}_\ell$, $\ell = 1, \dots, L$, obtained from the SOC observer.

The battery capacity estimation $\hat{Q}$ is obtained by the subsystem represented by the dashed block in the center of Fig. 2 which implements (6) with (18)–(19). The inputs of this subsystem are the battery current i_b and the state of charge $\hat{SOC}$ estimated by the observer.

The interconnection of the SOC observer (4) with the RLS algorithms used for the estimation of the battery capacity and the parameters of the $OCV(SOC)$ curve requires some modifications on the observer equations. The inputs of the SOC observer are the measured current i_b and voltage e_b, similarly as in (4), but for the entire scheme also the estimations of the parameters $\hat{Q}$, $\hat{\alpha}_p$, $p = 0, \dots, P$, and $\hat{\beta}_j$, $j = 0, \dots, J$, must be provided to the observer. In particular, the equations (4) of the ideal SOC observer are replaced by the following

$$\hat{v}_\ell(k) = \frac{R_\ell C_\ell}{h + R_\ell C_\ell}\hat{v}_\ell(k-1) + \frac{hR_\ell}{h + R_\ell C_\ell} i_b(k) + g_\ell(e_b(k) - \hat{e}_b(k)) \tag{21a}$$

$$\hat{SOC}(k) = \hat{SOC}(k-1) - \frac{h}{\hat{Q}(k)} i_b(k) + g_{L+1}(e_b(k) - \hat{e}_b(k)) \tag{21b}$$

$$\hat{e}_b(k) = \sum_{p=0}^{P} \hat{\alpha}_p(k)(\hat{SOC}(k))^p - \sum_{\ell=1}^{L} \hat{v}_\ell(k) - \sum_{j=0}^{J} \hat{\beta}_j(k)(\hat{SOC}(k))^j i_b(k) \tag{21c}$$

for $\ell = 1, \dots, L$, $k \in \mathbb{N}$, where the parameters $\hat{Q}(k)$, $\hat{\alpha}_p(k)$, $p = 0, 1, \dots, P$, $\hat{\beta}_j(k)$, $j = 0, \dots, J$, are obtained from the RLS algorithms described in the previous section.

A formal analysis of the possible convergence to zero of the estimation errors of the integrated estimator is nothing but easy due to the nonlinearity of the entire system, see (21b) where the inverse of $\hat{Q}$ appears, (21c) where the products of the parameters $\hat{\alpha}_p$ and $\hat{\beta}_j$ with the corresponding powers of $\hat{SOC}$ are present. On the other hand one can propose some rule of thumb for the design of the estimator gains. In particular, the vector g and the scalar μ can be chosen such that the dynamics of the SOC observer are faster than those of the RLS algorithms dedicated to the estimations of the battery capacity and the parameters of the $OCV(SOC)$ and $R_0(SOC)$ characteristics. Indeed, the SOC varies at each cycle while the variations of these maps are expected to be much slower and the battery capacity usually changes with hundreds of charging and discharging cycles.

B. Enabling conditions

The on-board operating conditions of a battery depend on a variety of aspects related to the specific application, loading scenarios and charging strategies. Not all conditions though determine useful information for the identification process. This concept is exploited in the design of the enabling logic parameters of the co-estimation framework proposed in this paper, which are activated under specific operating conditions of interest for the estimation problem at hand. The enabling conditions are determined by exploiting measured variables (or their direct elaborations), i.e., without using the estimated variables.

In order to define the enabling conditions of the estimator let us define the following logic variables

$$\delta_1(k) = \begin{cases} 1 & \text{if } |i_b(k)| > \Delta_1 \\ 0 & \text{otherwise} \end{cases} \tag{22a}$$

$$\delta_2(k) = \begin{cases} 1 & \text{if } \left| i_b(k) - \frac{1}{N} \sum_{s=k-N+1}^{k} i_b(s) \right| < \Delta_2 \\ 0 & \text{otherwise} \end{cases} \tag{22b}$$

$$\delta_3(k) = \begin{cases} 1 & \text{if } \Delta_3^- < \left| e_b(k) - \frac{1}{N} \sum_{s=k-N+1}^{k} e_b(s) \right| < \Delta_3^+ \\ 0 & \text{otherwise} \end{cases} \tag{22c}$$

where $\delta_i \in \{0, 1\}$, $i = 1, 2, 3$, Δ_1, Δ_2, Δ_3^- and Δ_3^+ are positive real numbers which represent suitable thresholds to be calibrated.

The RLS estimators of the parameters $\hat{\alpha}_p$, $p = 0, \dots, P$, $\hat{\beta}_j$, $j = 0, \dots, J$, and $\hat{Q}$ are activated only if the three logic conditions are contemporary true, i.e., $\delta = \delta_1 \delta_2 \delta_3 = 1$, see (6). The SOC estimation is disabled only when the battery current is zero, but the internal voltage is estimated in this situation too in order to capture the dynamics of the relaxation phases. When an estimator is disabled, the corresponding estimated variables are kept equal to their values at the previous time-step.

The logic variable δ_1 in (22a) is zero if the absolute value of the current is below a small threshold Δ_1. The logic variable δ_2 in (22b) is nonzero when the absolute value of the difference between the current and its moving average is below the threshold Δ_2. The condition allows one to exclude situations when large current variations over short time intervals occur. Finally, the estimator does not perform any operations also if it is not compliant with the condition expressed by (22c), i.e., the difference between the instantaneous voltage and its moving average must belong to the interval (Δ_3^-, Δ_3^+). This condition is adopted for excluding the computation when large variations of the voltage occur, e.g., at the beginning of the relaxation phases. Moreover, since $\Delta_3^- > 0$, the condition (22c) disables the estimator also when the voltage is constant, corresponding to having small variations in SOC.

V. Estimation Results

The effectiveness of the proposed integrated estimator is verified over experimental data collected for a cylindrical LG M50T INR21700 Li-ion cell with NMC cathode chemistry, nominal voltage 3.63 V, nominal capacity $Q^* = 4.85$ A h. Experiments were carried out at the Stanford Energy Control Laboratory in the Energy Resources Engineering Department at Stanford University. The experimental setup used for the aging campaign is composed of the Arbin LBT21024 battery cycler with a programmable power supply and an electronic load; a MITS Pro data acquisition software for the programming of test profiles and the environmental chamber AMEREX

IC500R. Tests were performed at controlled temperature of 25 °C [39].

A. Aging campaign

The aging campaign consists in subjecting the battery to a real driving profile - in the form of Urban Dynamometer Driving Schedule (UDDS). Periodic characterization tests, i.e., Capacity test and Hybrid Pulse Power Characterization (HPPC) test, were performed to assess battery health.

The battery is charged by using the constant current-constant voltage ($CC-CV$) standard charging protocol. Each iteration of the aging test starts with a $C/4$ discharge to bring the battery from $SOC = 1$ down to $SOC = 0.8$. Then, a UDDS driving cycle is implemented until the state of charge reaches $SOC = 0.2$. The current and voltage profiles for this sequence of operations at the beginning of the aging campaign are shown in Fig. 3. The current and voltage profiles after 200 cycles are the same except for the initial CC phase which is much shorter, i.e., a duration of 2565 s for the fresh battery and 45 s for the aged one.

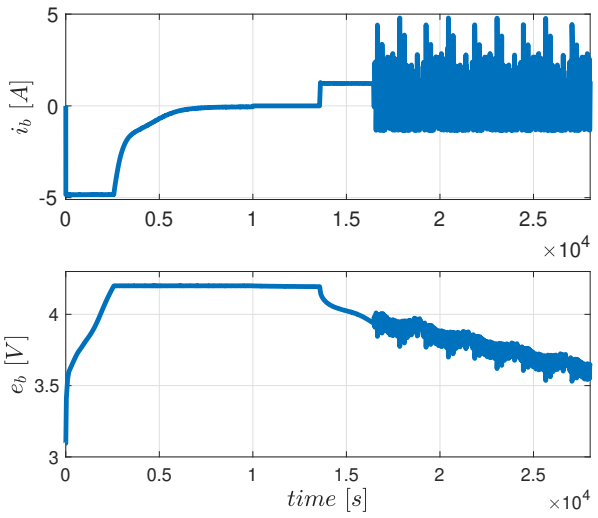

Fig. 3. Current i_b (top) and voltage e_b (bottom) for the first part of the aging campaign which consists of the following sequence: $CC-CV$ charging, discharge at $C/4$ rate, UDDS driving cycle.

Every 50 aging cycles a Capacity test and an HPPC test are performed. The former consists of a $C/20$ constant discharge whereas the latter consists of charge and discharge pulses at different SOC. Each aging test is completed with a sequence of a charging with constant current at $3C$ and a constant voltage at 4 V, up to $SOC = 0.8$ followed by a charging with constant current at $C/4$ and a constant voltage at 4.2 V until the battery is fully charged.

B. Benchmarks and parameters tuning

The benchmark values of the battery capacity have been obtained by using the capacity tests during the aging campaign. The values obtained for the battery under test are $Q = 4.85$ A h at the beginning of the battery life and $Q = 4.65$ A h after 200 cycles. The HPPC test is used for the determination of the benchmark values of the ECM parameters. The $R_0(SOC)$ maps for the fresh battery and after cycling are obtained by computing the voltage discontinuities in correspondence to the step changes of the current for different values of SOC. The results are shown in Fig. 7 with stars. It should be noticed that the data used for the determination of these maps are excluded from the set of data exploited by the online estimator by means of the logic variable δ_3 in (22). The values $R_1 = 0.03\,\Omega$ and $C_1 = 1.15$ kF are obtained by implementing the strategy discussed in Subsection III-E during the relaxation phases of the HPPC tests where the estimations of the other parameters are disabled by the logic variable δ_1 which is zero. The benchmark $OCV(SOC)$ maps are obtained by implementing charging and discharging tests at very small current, i.e., $C/20$, at the beginning of the battery life ad after 200 cycles.

The main parameters to be tuned for the proposed method are the thresholds Δ_1, Δ_2, Δ_3^- and Δ_3^+ used for defining the logic variables δ_1, δ_2 and δ_3 in (22). The value of Δ_1 is chosen such that currents below a value which determine negligible SOC variations are neglected. In our case we have chosen $\Delta_1 = 0.01$ A. The value of Δ_2 can be tuned by considering a current step change of sufficiently small amplitude Δ, e.g., 10% of the 1C current. In this case the inequality (22b) becomes $\Delta\left(1-\frac{k}{N}\right) \leq \Delta_2$ and one can fix Δ_2 by choosing a certain fraction of time-steps which could be missed without loosing relevant information from measurements. In our case we have chosen $\Delta_2 = 0.15$ A. The threshold Δ_3^+ can be calibrated similarly to Δ_2 by considering a step change Δ equal to 10% of the minimum voltage of the $OCV(SOC)$ map and the corresponding inequality (22c), which lead in our case to $\Delta_3^+ = 0.05$ V. The value of Δ_3^- is fixed by considering the voltage measurement accuracy which in our case lead to $\Delta_3^- = 0.003$ V. A sensitivity analysis for the chosen thresholds around their nominal values has been carried out showing a good robustness of the proposed tuning procedure. It should be noticed that during the validation tests the thresholds for (22) are kept the same.

The other estimator parameters are: $g_1 = 0.5$, $g_2 = 0.001$, $\mu = 0.99$ for both the RLS estimators, $P = 5$, $J = 2$, and all matrices $S(0)$ equal to identity matrices with suitable dimensions. All initial conditions of the estimated variables are assigned equal to zero unless otherwise noted.

C. UDDS driving cycle

The validation test is obtained by considering a UDDS driving cycle whose corresponding electrical variables are reported in the discharge phase of Fig. 3. In this test the current demanding to the battery system has a more practical profile with respect to the standard CC/CV charging protocol. The scope is to validate the effectiveness of the proposed estimator especially in these more complex situations.

The estimator is run for the new battery and after 200 cycles. Figure 4 shows the time evolution of the battery voltage error $e_b - \hat{e}_b$ in the two cases. Note that different time instants where the UDDS driving cycle starts for the two experiments have been considered to avoid overlapping the curves of the estimated parameters. The RMS of the voltage errors are $4.6\cdot$

10^{-6} and $5.4 \cdot 10^{-6}$, respectively. Figure 5 shows the estimated SOC when an initial estimation error of 80% at the beginning of the UDDS cycle is considered, i.e. $\hat{SOC}(0) = 0.2$ and the battery starts at full charge. The RMS of the SOC estimation errors are $5.4 \cdot 10^{-6}$ when the battery is fresh and $7.2 \cdot 10^{-5}$ after aging.

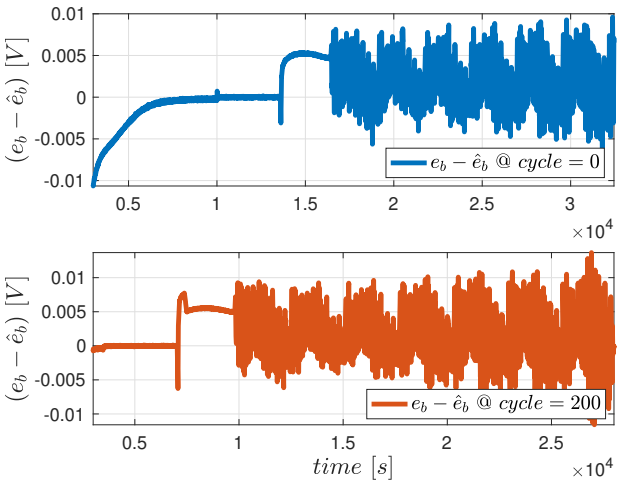

Fig. 4. Error between the measured voltage e_b and the estimated voltage $\hat{e}_b$ at the beginning of the battery life (top) and after 200 cycles (bottom) for the UDDS driving cycle test.

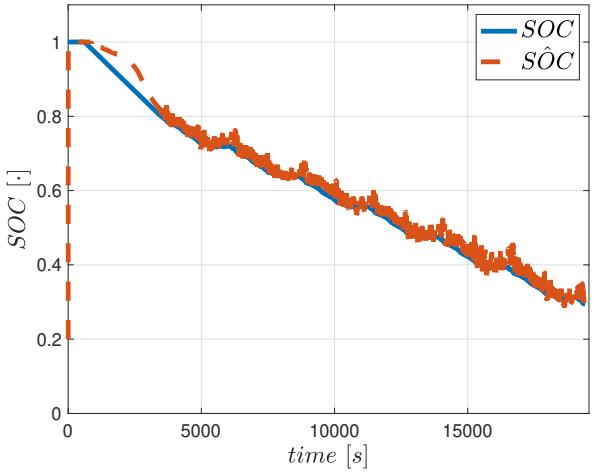

Fig. 5. Real (blue, continuous) and estimated (red, dashed) state of charge for the UDDS test after 200 cycles.

Figure 6 shows the effectiveness of the proposed battery capacity estimation also starting with different initial conditions. For the case after 200 cycles the enabling conditions are zero for a longer initial time interval because of the much shorter CC phase. The convergence time evaluated when the enabling conditions are active is about $150\,\mathrm{s}$ for all tests. The steady-state errors of the estimated capacities with respect to the benchmarks is less than $0.02\,\mathrm{A\,h}$, i.e., 0.44% in all scenarios, thus confirming the accuracy and the robustness of the estimations.

The estimated quadratic functions which approximate the $R_0(SOC)$ maps are shown in Fig. 7. The initial conditions of the estimator are $\hat{\beta}_j(0) = 0, j = 0, 1, 2$. The RMS errors of the estimated values with respect to the corresponding benchmarks obtained from the HPPC tests are $2.2 \cdot 10^{-3}$ for the fresh battery and $6.9 \cdot 10^{-3}$ after aging.

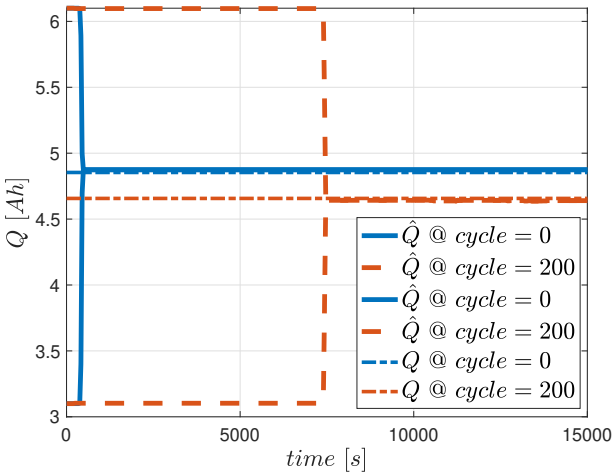

Fig. 6. Battery capacity $\hat{Q}$ for the UDDS driving cycle test evaluated with initial conditions $\hat{Q}(0) = 3.1\,\mathrm{A\,h}$ and $\hat{Q}(0) = 6.1\,\mathrm{A\,h}$ at the beginning of battery life (blue, continuous) and after 200 cycles (red, dashed), for the UDDS driving cycle test. The corresponding benchmark values are represented with dashed-dotted lines, blue and red, respectively.

The approximation of the $OCV(SOC)$ map is chosen with a fifth order polynomial with initial conditions $\hat{\alpha}_0(0) = 2.6\,\mathrm{V}$ and $\hat{\alpha}_p(0) = 0$, $p = 1, \ldots, 5$. The parameters estimation captures the variation of the $OCV(SOC)$ due to the battery aging, so as shown in Fig. 8. The RMS error of the polynomial approximations are $5.9 \cdot 10^{-3}$ when the battery is fresh and $1.5 \cdot 10^{-2}$ after aging with 200 cycles.

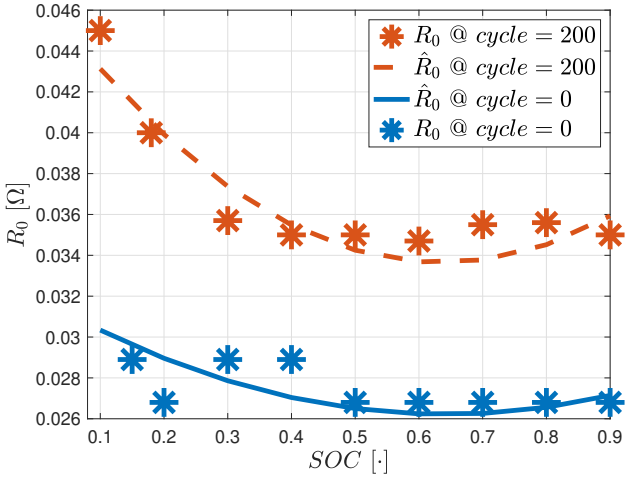

Fig. 7. Internal resistance characteristic $R_0(SOC)$ obtained with the UDDS driving cycle test at the beginning of battery life (blue) and after 200 cycles (red). The corresponding benchmark values are represented with stars, blue and red, respectively.

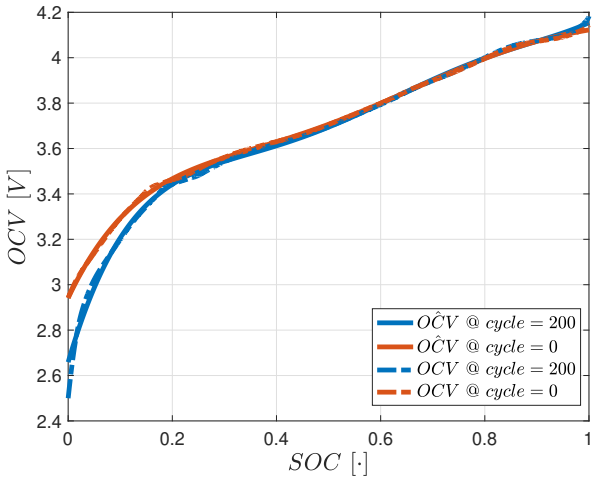

Fig. 8. $\hat{OCV}$ vs SOC evaluated at the beginning of battery life (blue, continuous) and after 200 cycles (red, dashed), for the UDDS driving cycle test. The corresponding benchmark values are represented with dashed-dotted lines, blue and red, respectively.

D. Performance comparison

The effectiveness of the proposed strategy is shown through a comparison with the co-estimation technique proposed in [18]. The estimated R_1 and C_1 are practically the same as those we obtained with the technique described in Subsection III-E. Table I summarizes the results for a performance comparison. In particular, four tests with the UDDS driving cycle have been carried out: fresh (first and second rows) and aged (third and fourth rows) battery; our approach (first and third rows) and the comparative technique (second and fourth rows in light grey). The performance indices are the following: π_1 is the RMS error for the SOC estimation; π_2 and π_3 are the convergence time and the RMS error, respectively, of the estimated internal resistance; π_4 is the RMS error for the estimation of the $OCV(SOC)$ map; π_5 is the percentage relative error for the estimated battery capacity.

TABLE I
PERFORMANCE COMPARISON (SEE THE COMMENT ON THE TABLE FOR THE NOMENCLATURE).

π_1	π_2	π_3	π_4	π_5
$5.4 \cdot 10^{-6}$	1521 s	$2.2 \cdot 10^{-3}$	$5.9 \cdot 10^{-3}$	0.4%
$5.6 \cdot 10^{-6}$	1527 s	$2.9 \cdot 10^{-3}$	–	–
$7.2 \cdot 10^{-5}$	1521 s	$6.9 \cdot 10^{-3}$	$1.5 \cdot 10^{-2}$	0.2%
$7.0 \cdot 10^{-5}$	1577 s	$31.0 \cdot 10^{-3}$	$4.4 \cdot 10^{-2}$	4.7%

The values of π_1 show that the estimations of SOC obtained with the two strategies are very close in both scenarios due to the similar structure of the SOC observer used in the two techniques. The most important advantage of the proposed approach for a fresh battery (first and second rows of Table I) is the fact that in our framework the $OCV(SOC)$ characteristic and the capacity are estimated online while the benchmark values are used for implementing the comparative technique, i.e., π_4 and π_5 in the second row are null. The superiority of our technique becomes more evident in the presence of variations of the parameters due to aging and battery usage (third and fourth rows of Table I): the SOC estimation error π_1 is practically the same while all the other indices π_i, $i = 2, \ldots, 5$, are much better with our approach.

The advantages of using the proposed enabling conditions has been verified during a charging phase. In particular, without (22) an increase of more than 60% of the convergence time for the parameters of the $OCV(SOC)$ and $R_0(SOC)$ characteristics is obtained.

VI. CONCLUSION

The co-estimation of SOC together with the battery capacity, the $OCV(SOC)$ and $R_0(SOC)$ maps and the other ECM parameters are key for any effective battery management strategy. In this paper, we have proposed an integrated estimation strategy which combines a model based SOC observer and RLS techniques for the estimation of the battery model parameters. The algorithm is activated by logic conditions aimed at capturing the operating conditions of interest for the estimation procedure. The use of moving average functions in the enabling strategy allows one to rule out the operating conditions in which the current is too small or large current variations appear in a very short time interval and/or the battery relaxation phenomenon occurs. Experimental data have been used to show the effectiveness of the proposed solution for realistic driving cycles over battery life. Future research will focus on extending the proposed strategy by considering the thermal effects too and the explicit dependence of the internal resistance on current rate and frequency.

REFERENCES

[1] G. L. Plett, "Recursive approximate weighted total least squares estimation of battery cell total capacity," J. of Power Sources, vol. 196, no. 4, pp. 2319–2331, 2011.
[2] M. Berecibar, I. Gandiaga, I. Villarreal, N. Omar, J. Van Mierlo, and P. Van den Bossche, "Critical review of state of health estimation methods of Li-ion batteries for real applications," Renewable and Sustainable Energy Reviews, vol. 56, pp. 572–587, 2016.
[3] Energy Vehicle Technologies Program, U.S. Department of Energy, "United States Advanced Battery Consortium Battery Test Manual For Electric Vehicles," INL/EXT-15-34184, 2020.
[4] J. Tian, R. Xiong, and Q. Yu, "Fractional-Order Model-Based Incremental Capacity Analysis for Degradation State Recognition of Lithium-Ion Batteries," IEEE Trans. on Industrial Electronics, vol. 66, no. 2, pp. 1576–1584, 2019.
[5] A. Farmann and D. U. Sauer, "A study on the dependency of the open-circuit voltage on temperature and actual aging state of lithium-ion batteries," J. of Power Sources, vol. 347, pp. 1–13, 2017.
[6] T. Ouyang, P. Xu, J. Lu, X. Hu, B. Liu, and N. Chen, "Coestimation of State-of-Charge and State-of-Health for Power Batteries Based on Multithread Dynamic Optimization Method," IEEE Trans. on Industrial Electronics, vol. 69, no. 2, pp. 1157–1166, 2022.
[7] H. Rahimi-Eichi, F. Baronti, and M.-Y. Chow, "Online Adaptive Parameter Identification and State-of-Charge Coestimation for Lithium-Polymer Battery Cells," IEEE Trans. on Industrial Electronics, vol. 61, no. 4, pp. 2053–2061, 2013.
[8] C. Zhang, X. Li, W. Chen, G. G. Yin, and J. Jiang, "Robust and adaptive estimation of state of charge for Lithium-ion batteries," IEEE Trans. on Industrial Electronics, vol. 62, no. 8, pp. 4948–4957, 2015.
[9] A. Klintberg, C. Zou, B. Fridholm, and T. Wik, "Kalman filter for adaptive learning of two-dimensional look-up tables applied to OCV-curves for aged battery cells," Control Engineering Practice, vol. 84, pp. 230–237, 2019.

[10] L. Lavigne, J. Sabatier, J. M. Francisco, F. Guillemard, and A. Noury, "Lithium-ion Open Circuit Voltage (OCV) curve modelling and its ageing adjustment," J. of Power Sources, vol. 324, pp. 694–703, 2016.

[11] K. Li, F. Wei, K.-J. Tseng, and B.-H. Soong, "A practical lithium-ion battery model for state of energy and voltage responses prediction incorporating temperature and ageing effects," IEEE Trans. on Industrial Electronics, vol. 65, no. 8, pp. 6696–6708, 2018.

[12] D.-I. Stroe, M. Swierczynski, S. K. Kær, and R. Teodorescu, "Degradation behavior of lithium-ion batteries during calendar ageing – The case of the internal resistance increase," IEEE Trans. on Industry Applications, vol. 54, no. 1, pp. 517–525, 2017.

[13] V.-H. Duong, H. A. Bastawrous, K. Lim, K. W. See, P. Zhang, and S. X. Dou, "Online state of charge and model parameters estimation of the LiFePO4 battery in electric vehicles using multiple adaptive forgetting factors recursive least-squares," J. of Power Sources, vol. 296, pp. 215–224, 2015.

[14] H. Rahimi-Eichi, F. Baronti, and M.-Y. Chow, "Online Adaptive Parameter Identification and State-of-Charge Coestimation for Lithium-Polymer Battery Cells," IEEE Trans. on Industrial Electronics, vol. 61, no. 4, pp. 2053–2061, 2014.

[15] Y. Gao, K. Liu, C. Zhu, X. Zhang, and D. Zhang, "Co-Estimation of State-of-Charge and State-of-Health for Lithium-Ion Batteries Using an Enhanced Electrochemical Model," IEEE Trans. on Industrial Electronics, vol. 69, no. 3, pp. 2684–2696, 2022.

[16] G. L. Plett, Battery management systems, Volume II: Equivalent-circuit methods. Artech House, 2015.

[17] Y. Wang, J. Tian, Z. Sun, L. Wang, R. Xu, M. Li, and Z. Chen, "A comprehensive review of battery modeling and state estimation approaches for advanced battery management systems," Renewable and Sustainable Energy Reviews, vol. 131, p. 110015, 2020.

[18] Z. Wei, G. Dong, X. Zhang, J. Pou, Z. Quan, and H. He, "Noise-Immune Model Identification and State-of-Charge Estimation for Lithium-Ion Battery Using Bilinear Parameterization," IEEE Trans. on Industrial Electronics, vol. 68, no. 1, pp. 312–323, 2021.

[19] J. Meng, D.-I. Stroe, M. Ricco, G. Luo, and R. Teodorescu, "A Simplified Model-Based State-of-Charge Estimation Approach for Lithium-Ion Battery With Dynamic Linear Model," IEEE Trans. on Industrial Electronics, vol. 66, no. 10, pp. 7717–7727, 2019.

[20] Z. Wei, C. Zou, F. Leng, B. H. Soong, and K.-J. Tseng, "Online Model Identification and State-of-Charge Estimate for Lithium-Ion Battery With a Recursive Total Least Squares-Based Observer," IEEE Trans. on Industrial Electronics, vol. 65, no. 2, pp. 1336–1346, 2018.

[21] F. Naseri, E. Schaltz, D.-I. Stroe, A. Gismero, and E. Farjah, "An Enhanced Equivalent Circuit Model With Real-Time Parameter Identification for Battery State-of-Charge Estimation," IEEE Trans. on Industrial Electronics, vol. 69, no. 4, pp. 3743–3751, 2021.

[22] H. Chaoui, N. Golbon, I. Hmouz, R. Souissi, and S. Tahar, "Lyapunov-based adaptive state of charge and state of health estimation for Lithium-ion batteries," IEEE Trans. on Industrial Electronics, vol. 62, no. 3, pp. 1610–1618, 2015.

[23] Y. Zou, X. Hu, H. Ma, and S. E. Li, "Combined State of Charge and State of Health estimation over lithium-ion battery cell cycle lifespan for electric vehicles," J. of Power Sources, vol. 273, pp. 793–803, 2015.

[24] M. Gholizadeh and F. R. Salmasi, "Estimation of State of Charge, Unknown Nonlinearities, and State of Health of a Lithium-Ion Battery Based on a Comprehensive Unobservable Model," IEEE Trans. on Industrial Electronics, vol. 61, no. 3, pp. 1335–1344, 2013.

[25] W. Yan, B. Zhang, G. Zhao, S. Tang, G. Niu, and X. Wang, "A Battery Management System With a Lebesgue-Sampling-Based Extended Kalman Filter," IEEE Trans. on Industrial Electronics, vol. 66, no. 4, pp. 3227–3236, 2018.

[26] Y. Feng, C. Xue, Q.-L. Han, F. Han, and J. Du, "Robust Estimation for State-of-Charge and State-of-Health of Lithium-Ion Batteries Using Integral-Type Terminal Sliding-Mode Observers," IEEE Trans. on Industrial Electronics, vol. 67, no. 5, pp. 4013–4023, 2019.

[27] S. Li, K. Li, E. Xiao, and C.-K. Wong, "Joint SoC and SoH Estimation for Zinc–Nickel Single-Flow Batteries," IEEE Trans. on Industrial Electronics, vol. 67, no. 10, pp. 8484–8494, 2020.

[28] C. Zou, X. Hu, S. Dey, L. Zhang, and X. Tang, "Nonlinear Fractional-Order Estimator With Guaranteed Robustness and Stability for Lithium-Ion Batteries," IEEE Trans. on Industrial Electronics, vol. 65, no. 7, pp. 5951–5961, 2018.

[29] X. Hu, H. Yuan, C. Zou, Z. Li, and L. Zhang, "Co-Estimation of State of Charge and State of Health for Lithium-Ion Batteries Based on Fractional-Order Calculus," IEEE Trans. on Vehicular Technology, vol. 67, no. 11, pp. 10 319–10 329, 2018.

[30] R. Xiong, J. Wanga, W. Shen, J. Tian, and H. Mua, "Co-Estimation of State of Charge and Capacity for Lithium-Ion Batteries with Multi-Stage Model Fusion Method," Engineering, vol. 7, pp. 1469–1482, 2021.

[31] D. Xiao, G. Fang, S. Liu, S. Yuan, R. Ahmed, S. Habibi, and A. Emadi, "Reduced-Coupling Coestimation of SOC and SOH for Lithium-Ion Batteries Based on Convex Optimization," IEEE Trans. on Power Electronics, vol. 35, no. 11, pp. 12 332–12 346, 2020.

[32] X. Hu, H. Jiang, F. Feng, and B. Liu, "An enhanced multi-state estimation hierarchy for advanced lithium-ion battery management," Applied Energy, vol. 257, p. 114019, 2020.

[33] R. Xiong, H. He, F. Sun, and K. Zhao, "Evaluation on State of Charge Estimation of Batteries With Adaptive Extended Kalman Filter by Experiment Approach," IEEE Trans. on Vehicular Technology, vol. 62, no. 1, pp. 108–117, 2013.

[34] P. Shen, M. Ouyang, L. Lu, J. Li, and X. Feng, "The Co-estimation of State of Charge, State of Health, and State of Function for Lithium-Ion Batteries in Electric Vehicles," IEEE Trans. on Vehicular Technology, vol. 67, no. 1, pp. 92–103, 2018.

[35] S. Zhang and X. Zhang, "A multi time-scale framework for state-of-charge and capacity estimation of lithium-ion battery under optimal operating temperature range," J. of Energy Storage, vol. 35, p. 102325, 2021.

[36] S. Zhang, X. Guo, and X. Zhang, "A novel one-way transmitted co-estimation framework for capacity and state-of-charge of lithium-ion battery based on double adaptive extended Kalman filters," J. of Energy Storage, vol. 33, p. 102093, 2021.

[37] L. Iannelli, K. H. Johansson, U. T. Jönsson, and F. Vasca, "Averaging of nonsmooth systems using dither," Automatica, vol. 42, no. 4, pp. 669–676, 2006.

[38] L. Iannelli, K. H. Johansson, U. T. Jönsson, and F. Vasca, "Subtleties in the averaging of a class of hybrid systems with applications to power converters," Control Engineering Practice, vol. 16, no. 8, pp. 961–975, 2008.

[39] G. Pozzato, A. Allam, and S. Onori, "Lithium-ion battery aging dataset based on electric vehicle real-driving profiles," Data in Brief, vol. 41, p. 107995, 2022.

Domenico Natella accomplished the Master's Degree cum laude in Software Engineering at the University of Sannio, Italy, in 2018. Since December 2018 he has been a Ph.D. student at the same university. His research interests include battery management system and reinforcement learning.

Simona Onori received the Laurea degree in computer science and engineering from the University of Rome "Tor Vergata" Italy, in 2003, the M.S. degree in electronics and communications engineering from The University of New Mexico, USA, in 2005, and the Ph.D. degree in control engineering from the University of Rome "Tor Vergata" in 2007. She is currently an Assistant Professor with the Energy Resources Engineering at Stanford University and Electrical Engineering (by courtesy). Dr. Onori is the recipient of the 2020 U.S. DOE C3E Award in the research category, 2019 Board of Trustees Award for Excellence, Clemson University, the 2018 Global Innovation Contest Award from LG Chem, the 2018 SAE Ralph R. Teetor Educational Award, and the 2017 NSF CAREER Award. She has been serving as the Editor-in-Chief for the SAE International Journal of Electrified Vehicles since 2020. She is a Distinguished Lecturer of the IEEE Vehicular Technology Society.

Francesco Vasca received the Ph.D. degree in Automatic Control from the University of Napoli Federico II, Italy, in 1995. Since 2015, he has been a Full Professor of Automatic Control with the Department of Engineering, University of Sannio, Benevento, Italy. His research interests include the analysis and control of switched and networked dynamic systems with applications to power electronics, railway control, automotive control and social networks. From 2008 to 2014 he has been an Associate Editor for the IEEE Transactions on Control Systems Technology and since 2017 he serves as Associate Editor for Automatica.